Finite driving rate and anisotropy effects in landslide modeling

E. Piegari, V. Cataudella, R. Di Maio, L. Milano, and M. Nicodemi
Dipartimento di Scienze Fisiche, Università di Napoli "Federico II," INFM-Coherentia and INFN, Napoli, Italy
(Received 26 July 2005; published 21 February 2006)

In order to characterize landslide frequency-size distributions and individuate hazard scenarios and their possible precursors, we investigate a cellular automaton where the effects of a finite driving rate and the anisotropy are taken into account. The model is able to reproduce observed features of landslide events, such as power-law distributions, as experimentally reported. We analyze the key role of the driving rate and show that, as it is increased, a crossover from power-law to non-power-law behaviors occurs. Finally, a systematic investigation of the model on varying its anisotropy factors is performed and the full diagram of its dynamical behaviors is presented.

DOI: 10.1103/PhysRevE.73.026123 PACS number(s): 05.65.+b, 91.30.Px

I. INTRODUCTION

Over the last two decades, the evidence of power laws in frequency-size distributions of several natural hazards such as earthquakes [1], volcanic eruptions [2], forest fires [3–5], and landslides [5,6] has suggested a relationship between these complex phenomena and self-organized criticality (SOC) [7]. The idea of SOC [8], applied to many media exhibiting avalanche dynamics [9,10], refers to the tendency of natural systems to self-organize into a critical state where the distribution of event sizes is represented by a power law with an exponent α, which is universal in the sense that it is robust to minor changes in the system. Generally, the nature of a *critical* state is evidenced by the fact that the size of a disturbance to the system is a poor predictor of the system response. Let us consider storms as perturbations for natural slopes. Large storms can produce large avalanches, but also small storms sometimes can do it. On the other hand, small storms usually do not produce any avalanches, but also large storms may not cause any avalanching phenomena. Moreover, avalanches triggered by small storms can be larger than those triggered by large storms. The unpredictability of the sizes of such system responses to incremental perturbations and the observed power-law statistics could be an exhibition of self-organized critical behavior in most natural avalanches. However, the idea of understanding power-law distributions within the framework of SOC is not the only one. Recently, in order to reproduce the range of power-law exponents observed for landslides, some authors have introduced a two-threshold cellular automaton, which relates landslide dynamics to the vicinity of a breakdown point rather than to self-organization [11].

In this paper, we report on an accurate investigation of a cellular automaton model, which we have recently proposed to describe landslide events and, specifically, their frequency-size distributions [12]. In particular, we discuss the role of a finite driving rate and the anisotropy effects in our nonconservative system. It has been pointed out by several authors that the driving rate is a parameter that has to be fine-tuned to zero in order to observe criticality [13–15]. We notice that the limit of zero driving rate is only attainable in an ideal chain reaction; therefore, finite rates of external drives are essential ingredients in the analysis of the dynamics of real avalanche processes. We show that increasing the driving rate the frequency-size distribution of landslide events evolves continuously from a power-law (small driving rates) to an exponential (Gaussian) function (large driving rates). Interestingly, a crossover regime characterized by a maximum of the distribution at small sizes and a power-law decay at medium and large sizes is found in the intermediate range of values of the driving rate for a wide range of level of conservation. Power-law behaviors are robust even though their exponents depend on the system parameters (e.g., driving rate and level of conservation; see below).

Although the critical nature of landslides is not fully assessed and many authors believe that deviations from the power law appear to be systematic for small landslides data [16,17], results from several regional landslide inventories show robust power-law distributions of medium and large events with a critical exponent $\alpha \sim 2.5 \pm 0.5$ [6]. The variation in the exponents of landslide size distributions is larger than in the other natural hazards that exhibit scale-invariant size statistics [18]. Whether this variation of α is caused by scatter in the data or because different exponents are associated with different geology is an important open question, which we may contribute to address.

The model we analyze describes the evolution of a space- and time-dependent factor of safety field. The factor of safety (S) is defined as the ratio between resisting forces and driving forces. It is a complicate function of many dynamical variables (pore water pressure, lithostatic stress, cohesion coefficients, etc.) whose rate of change is crucial in the characterization of landslide events. A landslide event may include a single landslide or many thousands. We investigate frequency-size distributions of landslide events by varying the driving rate of the factor of safety. Although our probability density distributions are lacking a direct comparison with frequency-size distributions of real landslides, they reproduce power-law scaling with an exponent very close to the observed values. Moreover, they allow us to get insight into the difficult problem of the determination of possible precursors of future events.

The paper is organized as follows. In the next section, we present the model and briefly discuss the differences between our approach and previous cellular automaton models that

have been recently introduced to characterize landslide frequency-size distributions. In Sec. III, we report numerical results obtained by a systematic investigation of the effects of a finite driving rate on the frequency-size distribution. The values of the exponent of the power-law decay are given as a function of the driving rate and the level of conservation. An accurate analysis of the spatial distribution of the values of the factor of safety by varying the driving rate provides useful information for quantifying hazard scenarios of possible avalanche events. In Sec. IV, we analyze the role of the anisotropic transfer coefficients, which control the propagation of the instability. We summarize our results in a phase diagram that shows the location of power-law and non-power-law scaling regions in the anisotropy parameter space. Conclusions are summarized in Sec. V.

II. THE MODEL

The instability in clays often starts from a small region, destabilizes the neighborhood, and then propagates [19]. Such a progressive slope failure recalls the spreading of avalanches in the fundamental models of SOC. The term "self-organized criticality" was coined by Bak, Tang, and Wiesenfeld to describe the phenomenon observed in a particular cellular automaton model, nowadays known as the sandpile model [8]. In the original sandpile model, the system is perturbed externally by a random addition of sand grains. Once the slope between two contiguous cells has reached a threshold value, a fixed amount of sand is transferred to its neighbors, generating a chain reaction or avalanche. The noncumulative number of avalanches, N_A, with area A satisfies a power-law distribution with a critical exponent $\alpha=1$ [20], which is much smaller than the values of the power-law exponents observed for landslides [5,6]. Few years later the paper of Bak *et al.* [8], Olami, Feder, and Christensen (OFC) recognized the dynamics of earthquakes as a physical realization of self-organized criticality and introduced a cellular automaton that gives a good prediction of the Gutenberg-Richter law [1]. Such a model, whose physical background belongs to the Burridge-Knopoff spring-block model [21], is based on a continuous dynamical variable which increases uniformly through time until it reaches a given threshold and relaxes. This means that the dynamical variable decreases, while a part of the loss is transferred to the nearest neighbors. If this transfer causes one of the neighbors to reach the threshold value, it relaxes too, resulting in a chain reaction. OFC recognized that the model still exhibits power-law scaling in the nonconservative regime, even if the power-law exponent strongly depends on the level of conservation.

In this paper, we investigate the role of a finite driving rate and of anisotropy in a nonconservative cellular automaton modeling landslides [12]. In such a model, we sketch a natural slope by using a square grid where each site i is characterized by a local value of the safety factor S_i. In slope stability analysis, the factor of safety, S, against slip is defined in terms of the ratio of the maximum shear strength τ_{max} to the disturbing shear stress τ:

$$S = \frac{\tau_{max}}{\tau}. \tag{1}$$

The limited amount of stress that a site can support is given by the empirical Mohr-Coulomb failure criterion: $\tau_{max}=c+(\sigma-u)\tan\phi$, where σ is the total normal stress, u is the pore-fluid pressure, ϕ is the angle of internal friction of the soil, and c is the cohesional (nonfrictional) component of the soil strength [22]. If $S>1$, resisting forces exceed driving forces and the slope remains stable. Slope failure starts when $S=1$. Since a natural slope is a complex nonhomogeneous system characterized by the presence of composite diffusion, dissipative, and driving mechanisms acting in the soil (such as those on the water content), we consider the time- and site-dependent safety factor S_i and treat the local inverse factor of safety, $e_i=1/S_i$, as the nonconserved dynamical variable of our cellular automaton model [12].

The long-term driving of the OFC model is, here, replaced by a dynamical rule which causes the increases of e_i through the time with a finite driving rate ν: $e_i(t+\Delta t)=e_i(t)+\nu\Delta t$. Such a rule allows us to simulate the effect on the factor of safety of different complex processes which can change the state of stress of a cell. The model is driven as long as $e_i<1$ on all sites i. Then, when a site—say, i—becomes unstable (i.e., exceeds the threshold, $e_{th}=1$) it relaxes with its neighbors according to the rule

$$e_i \to 0, \quad e_{nn} \to e_{nn} + f_{nn} e_i, \tag{2}$$

where nn denotes the nearest neighbors of site i and f_{nn} is the fraction of e_i toppling on nn. This relaxation rule is considered to be instantaneous compared to the time scale of the overall drive and lasts until all sites remain below the threshold. When e_i reaches the threshold value 1 and relaxes, the fraction of e_i moving from the site i to its "downward" ("upward") neighbor on the square grid is f_d (f_u), as $f_l=f_r$ is the fraction to each of its "left" and "right" neighbors. The transfer parameters f_{nn} are chosen in order to individuate a privileged transfer direction: we assume $f_u<f_d$ and $f_l=f_r<f_d$. We notice that the model reproduces features of the OFC model for earthquakes in the limit case $\nu=0$ and $f_{nn}=f \leqslant 0.25$. A detailed analysis of the model on varying the transfer coefficients f_{nn} is reported in Sec. IV.

Since many complex dissipative phenomena (such as evaporation mechanism, volume contractions, etc. [23]) contribute to a dissipative stress transfer in gravity-driven failures, we study the model in the nonconservative case $C=\Sigma_{nn} f_{nn}<1$, which makes our approach different from previous ones within the framework of SOC [18]. The conservation level C and the anisotropy factors, which we consider here to be uniform, are actually related to local soil properties (e.g., lithostatic, frictional, and cohesional properties), as well as to the local geometry of the slope (e.g., its morphology). The rate of change of the inverse factor of safety, ν, induced by the external drive (e.g., rainfall), in turn related to soil and slope properties, quantifies how the triggering mechanisms affect the time derivative of the S field.

Recently, in order to reproduce the range of the power-law exponents observed for landslides, several authors have used two-threshold cellular automata, which relate landslide dynamics to self-organization [24] or to the vicinity of a breakdown point [11]. In the first approach [24], a time-dependent criterion for stability, with a not easy interpretation in terms of governing physics, provides a power-law exponent close to 2 without any tuning. Therefore, this ap-

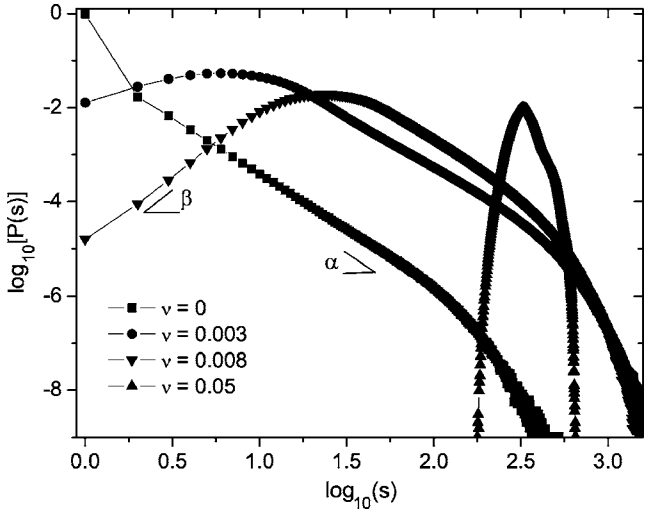

FIG. 1. Noncumulative frequency-size distributions on a 64 $\times$64 grid corresponding to four values of the driving rate. The logarithm of the normalized number of model events, $\log_{10}[P(s)]$, in which a specified number of different cells, s, become unstable, is given as a function of $\log_{10}(s)$. We show the case $C=0.4$, $f_u/f_d=2/3$, and $f_l/f_d=5/6$.

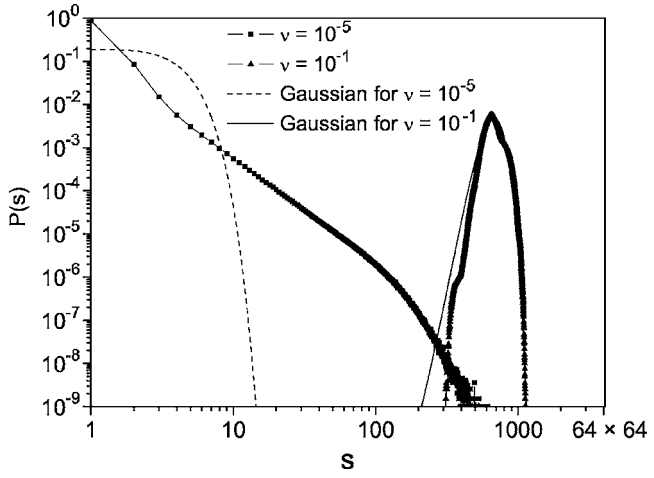

FIG. 2. Noncumulative frequency-size distributions and corresponding Gaussian distributions on a 64×64 grid for two values of the driving rate. Squares and triangles show the normalized number of model events, $P(s)$, in which a specified number of different cells, s, become unstable as a function of s. The dashed and solid lines are Gaussian distributions obtained for the same mean value and the standard deviation of the frequency-size distributions. We consider the case $C=0.4$, $f_u/f_d=2/3$, and $f_l/f_d=5/6$.

proach does not explain the observed variability of α. In Ref. [11], the range of α is found by tuning the maximum value of the ratio between the thresholds of two failure modes: the shear failure and the slab failure. However, the frequency-size distribution of avalanches is obtained by counting only clusters where shear failures have occurred, considering conservative transfer processes between adjacent cells with a different number of nearest neighbors. In this paper, the investigation of our nonconservative cellular automaton is mainly devoted to the characterization of landslide event dynamics on varying the driving rate in order to analyze different hazard scenarios.

III. EFFECT OF A FINITE DRIVE ON FREQUENCY-SIZE DISTRIBUTIONS

Frequency-size distributions give the number of landslides (events) as a function of their size. In Fig. 1 we show the noncumulative frequency-size distributions obtained for different values of the driving rate in the anisotropic nonconservative case $C=0.4$, with $f_u/f_d=2/3$ and $f_l/f_d=5/6$. The curves are obtained for a square lattice of size 64×64. We considered both cylindrical (open along the vertical axis and periodical along the horizontal axis) and open boundary conditions, which we checked differ in the slopes of the distribution curves for less than 1%.

In the limit of vanishing driving rate, the distribution of events, $P(s)$, is similar to that of the two-dimensional isotropic OFC model for a fixed value of the level of conservation: a power law characterized by a critical exponent α, $P(s)\sim s^{-\alpha}$, followed by a system finite-size-dependent exponential cutoff [9]. As discussed in Ref. [12], by increasing the driving rate ν, the probability distribution develops a maximum, which shifts towards larger events with ν. On the left side of the maximum, a power-law decay, with exponent β (see the Fig. 1), seems to appear for small landslide sizes. However, the few available data do not allow to distinguish log-log linear shape and an exponential one [17]. On the right side of the maximum of the distribution, the power-law regime remains until, by increasing ν, the distribution continuously modifies in a bell-shaped curve. Figure 2 shows the crossover of the probability distribution from power-law to Gaussian on increasing the driving rate.

The behavior of the power-law exponents on varying ν is shown in Fig. 3. Interestingly, the values of the power-law exponent α are very close to those experimentally reported [5]. As one can see, α increases until the value of the driving rate sensitively modifies the shape of the distribution with the appearance of a maximum. We find that the regime with a nonmonotonic frequency-size distribution is robust to changes in system parameters. In particular, it can be found for $\nu\in[10^{-4},10^{-2}]$ in the whole range $C\in[0.4,0.8]$.

The values of the exponents α and β sensitively change by varying another important parameter of the model that is the level of conservation C, which represents the nonconservative redistribution of the load of failing cells. The effect of C at finite driving rate is comparable to that obtained at $\nu=0$ [1], as shown in Fig. 4 (see also Ref. [12]).

Let us come back to Fig. 1 in order to highlight the role of the driving rate in the characterization of landslide events. From the distributions of Fig. 1, we see that large events can have comparatively high probabilities in the power-law regime (i.e., at small driving rates ν) with respect to the Gaussian regime (i.e., larger ν). Such a feature could allow one to reproduce the observation that sometimes mild rainfalls produce landslides as large as those triggered by intense rainfalls. To underline the nonlinear behavior of the system with ν, in Fig. 5 we plot the sizes of avalanches with the same probability of occurrence for different values of the driving

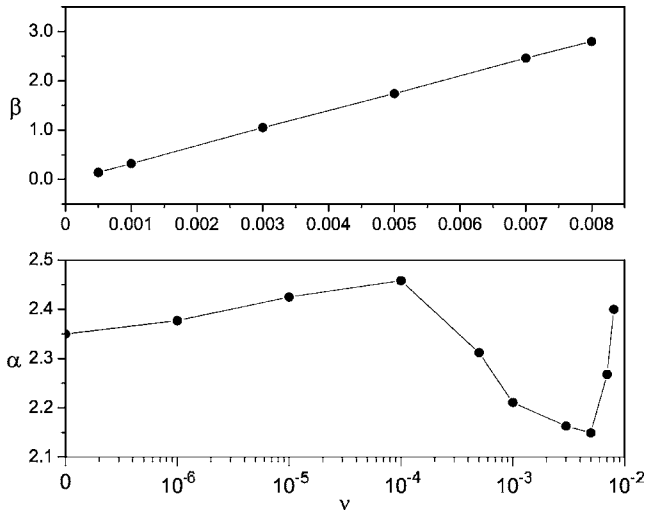

FIG. 3. Top: positive power-law exponent β as a function of the driving rate ν. Bottom: negative power-law exponent α as a function of ν. The values of the exponents are obtained for $C=0.4$, $f_u/f_d=2/3$, and $f_l/f_d=5/6$.

rate. Such sizes are the intersections of horizontal straight lines with the distribution curves of Fig. 1. When we consider small events [i.e., $P(s)$ as large as 10^{-2}], we find that the size of equiprobable events increases with the driving rate. Thus, for equiprobable events with high probability of occurrence the system response is essentially linear with the driving rate. Instead, for large events [i.e., $P(s)$ as small as 10^{-6}], the size of equiprobable events has a maximum as a function of ν. Thus, it appears that, for a given range of ν values, the size of events caused by a slow rate of changes of the factor of safety can be larger than the size of avalanches triggered by a faster rate. Moreover, an evidence is found for the existence of the most *dangerous* value of ν, for which the size of the system response has a maximum.

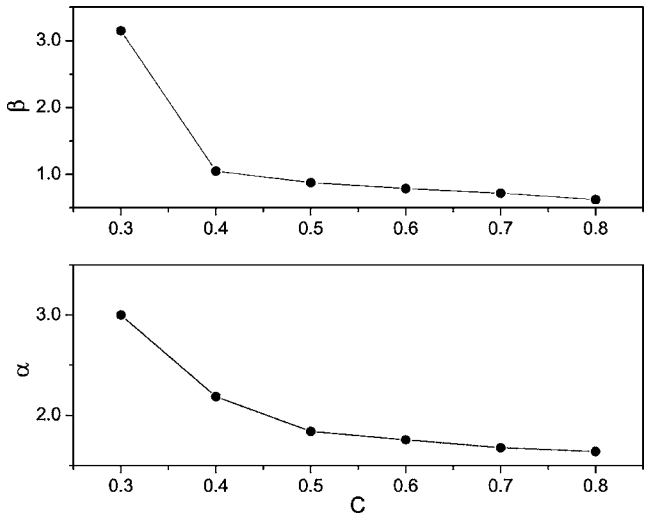

FIG. 4. Top: positive power-law exponent β as a function of the level of conservation C. Bottom: negative power-law exponent α as a function of C. The values of the exponents are obtained for $\nu=0.003$, $f_u/f_d=2/3$, and $f_l/f_d=5/6$.

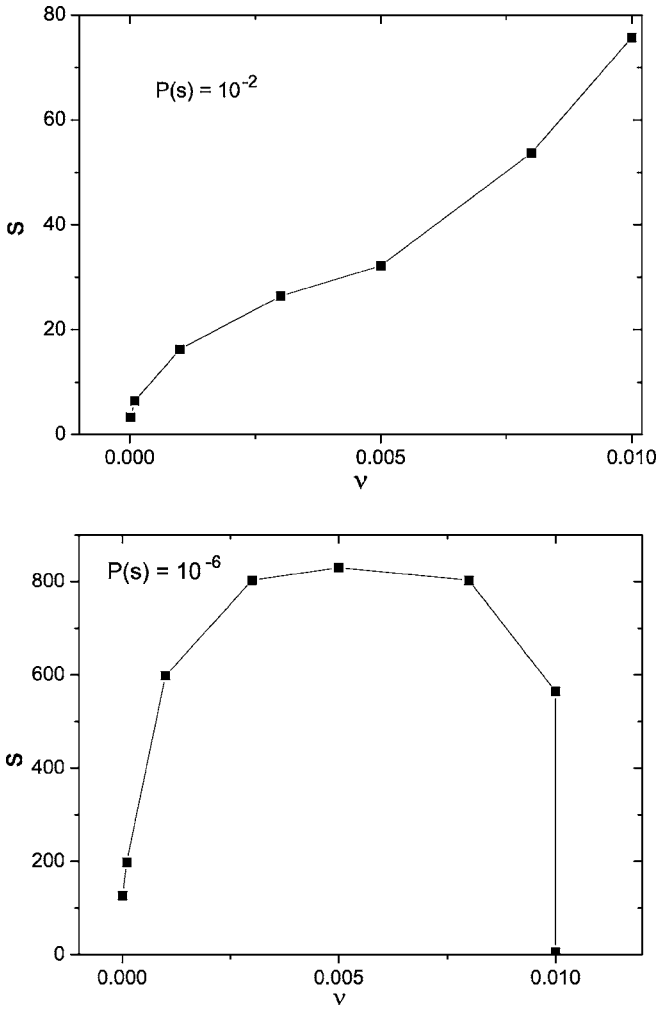

FIG. 5. Size s of equiprobable events (i.e., corresponding to the same probability of occurrence) as a function of the driving rate. Top: sizes of model events with $P(s)=10^{-2}$. Bottom: sizes of model events with $P(s)=10^{-6}$. In the top panel, only the largest sizes of equiprobable events are plotted.

Hazards scenarios

The detection of possible precursors of a landslide event is a crucial step to achieve hazard reduction. In order to get insight into this difficult problem, we visualize the structure of a typical landslide event for different values of the driving rate ν. In the top row of Fig. 6, we report on the 64×64 grid a typical avalanche of size $s=230$ on increasing the value of ν from left to right. The 230 black cells are those that have reached the instability threshold. As we can see, compact landslides are the characteristic response of a system governed by power-law statistics as happens at small ν (also when a maximum in the frequency-size distribution develops). Such a response is typical of systems with SOC behavior [26]. By increasing the driving rate, compact clusters survive until power-law regime disappears. As the system enters the non-power-law regime, the relevance of domino effects drastically drops and landslide events are characterized by many tiny independent clusters.

In the bottom row of Fig. 6, we show the distribution of the factor of safety, $S_i=1/e_i$, for the cases corresponding to

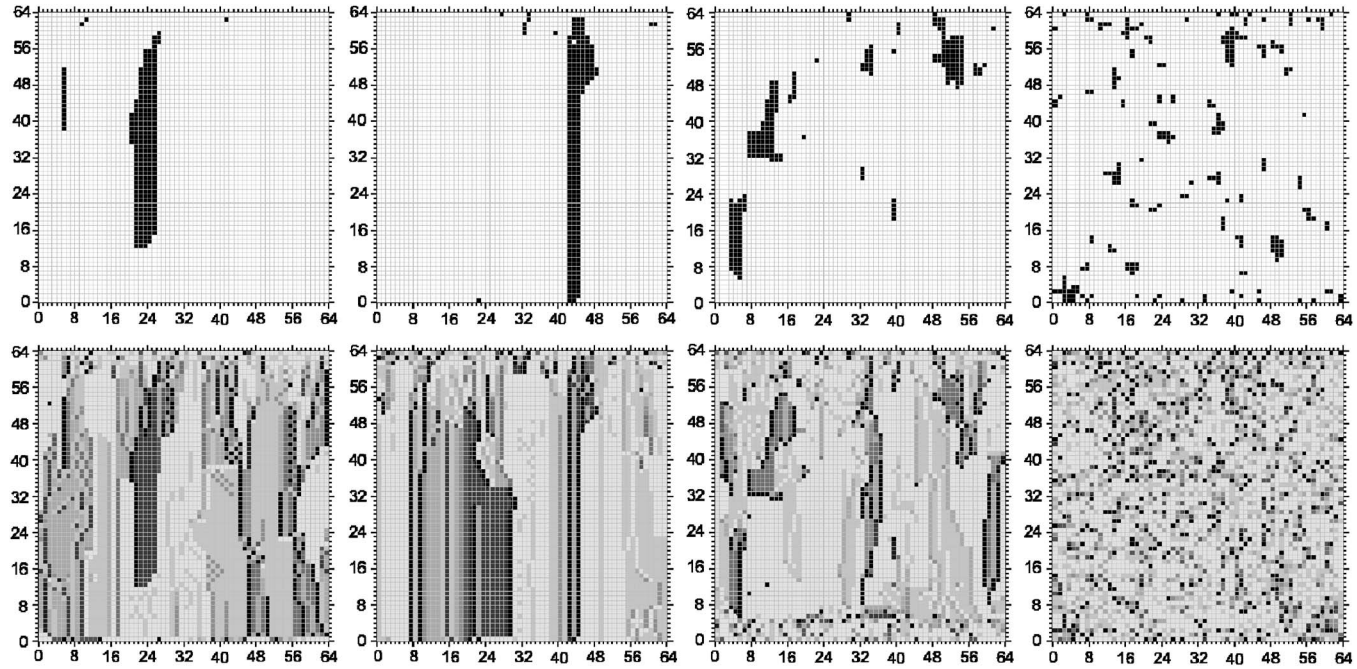

FIG. 6. Top row: snapshots of a landslide event of size $s=230$ on a 64×64 grid, for four values of the driving rate (from left to right): $\nu=10^{-5}$, $\nu=10^{-3}$, $\nu=5\times10^{-3}$, and $\nu=5\times10^{-2}$. The 230 black cells are those that have reached the instability threshold. The simulations are done in the case $C=0.4$, $f_u/f_d=2/3$, and $f_l/f_d=5/6$. Bottom row: snapshots of the factor of safety corresponding to the stable configurations reached after the avalanches shown in top row. The values of the factor of safety have been associated to ten levels of a gray scale from white to black, in order to measure the distance of a cell from its instability condition: the darker the color, the farther is the cell from the instability threshold.

the upper panels [25]. The distribution on the grid of the values shows how the spatial correlations in the system crucially affect landslide structures. In order to measure the distance of a cell from its instability condition and to visualize the correlated areas (regions with similar values of S_i), the values of S_i have been associated to ten levels of a gray scale from white to black: the darker the color, the farther is the cell from the instability threshold. In the snapshots of Fig. 6, it is possible to recognize as dark areas the avalanches shown in the corresponding upper grids. In particular, the dark areas typically are related to previous landslide events, whereas the lighter areas indicate regions of future events. We notice that in the power-law regime (i.e., small ν) even a very small perturbation (say, a drop of water) at one single point can trigger huge system responses. Instead, in the non-power-law regime (i.e., large ν) large-scale correlations are absent; here, large events trivially occur just because the strong external driving rate makes likely that many cells simultaneously approach the instability threshold. Thus, the detection of patterns of correlated domains in investigated areas results to be a crucial tool to identify the response of the system to perturbations, i.e., to hazard assessment.

It is worth noticing that the average value of the factor of safety on the grid cells $\langle S\rangle$ and its fluctuation $\langle\Delta S^2\rangle$ are very similar in the four cases showed in Fig. 6, encompassing a broad spectrum of ν values. Interestingly, the probability distribution of S on the grid sites, independently of the driving rate, is well approximated by a Gaussian distribution. This suggests that a measure of just an average safety factor on the investigated area could provide only a very partial information about the statistics governing the considered landslide events.

IV. ANISOTROPY EFFECTS ON FREQUENCY-SIZE DISTRIBUTIONS

In the previous sections, we have investigated the properties of the model on varying the driving rate ν at fixed values of the anisotropic ratios f_u/f_d and $f_l/f_d=f_r/f_d$. Such parameters control how the instability propagates downward and, therefore, they are complicate functions of the topography and geology of a specific area. In this section, we are interested in the analysis of the model when such transfer coefficients vary.

It is well known that the one-dimensional version of the sandpile and OFC models are characterized by non-power-law scaling [9]. Thus, we expect that, for small values of the ratio f_l/f_d, the frequency-size distribution does not show power-law behavior. Vice versa, for $f_u/f_d\sim1$ and $f_l/f_d\sim1$, we expect to have power-law distributions, as in the OFC model, which corresponds in our model to the limit $f=f_u=f_l=f_r=f_d$ and $\nu=0$.

The diagram of Fig. 7 summarizes the different regimes found in our simulations at fixed values of the driving rate $\nu=10^{-4}$ and the level of conservation $C=0.4$. We find that, on varying the anisotropic ratios, the parameter space is divided in three regions: (i) a power-law region (PL) characterized by power-law frequency-size distributions for large values of the anisotropic ratios, (ii) a non-power-law region (NPL) for the whole range of values of the anisotropic ratio

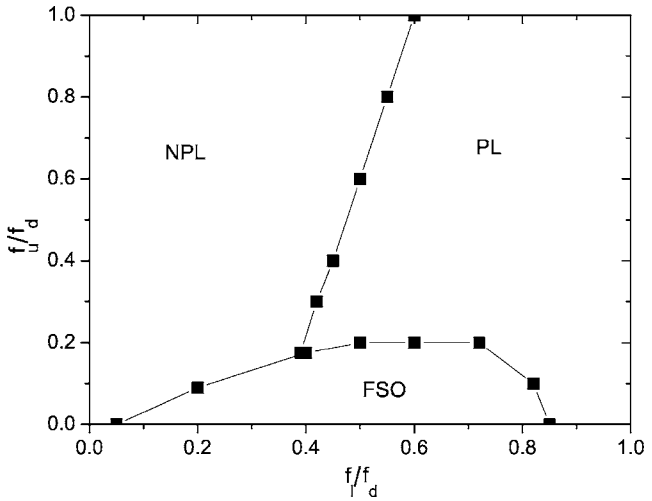

FIG. 7. Phase diagram in the f_u/f_d vs f_l/f_d plane. The lines divide the parameter space in to three regions: a power-law scaling region (PL), a non-power-law scaling region (NPL), and a finite-size oscillation region (FSO) where peaks of the distribution commensurate with the size of the grid appear. The results are obtained for $\nu=10^{-4}$ and $C=0.4$.

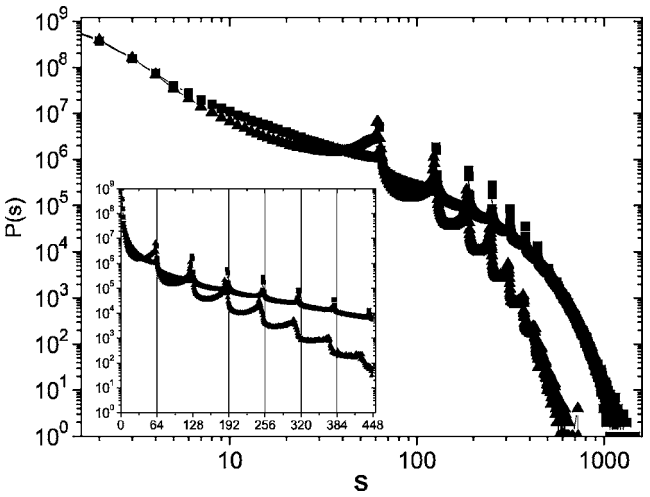

FIG. 8. Noncumulative frequency-size distributions on a 64 $\times 64$ grid for $f_u/f_d=0$ and $f_l/f_d=0.3$ (triangles) and $f_l/f_d=0.55$ (squares). The inset shows the distribution curves in a log-linear scale for the range of values where commensurate peaks are observed. The vertical lines mark multiples of the system size. The results are obtained for $\nu=10^{-4}$ and $C=0.4$.

f_u/f_d (which controls the redistribution of load in the vertical direction) and small values of f_l/f_d, and (iii) a finite-size oscillation region (FSO) where the frequency-size distribution is characterized by periodic peaks, which appear for integer multiples of the grid size $L=64$.

As expected, we find power-law and non-power-law behaviors for large and small values of the anisotropic ratios, respectively. In particular, we find that the value of the critical exponent α of the power-law distribution slightly increases with f_u/f_d for a fixed value of f_l/f_d and decreases with f_l/f_d for a fixed value of f_u/f_d. However, the changes in α are negligible.

It is worth noticing that, even if the ratio f_l/f_d is quite large, we find that the frequency-size distribution does not show a power-law decay when the value of f_u/f_d is small (see Fig. 7). Indeed, the probability distribution develops a finite number of peaks which are commensurate with the size of the grid. Figure 8 shows the frequency-size distribution for two different values of the anisotropic ratios in the FSO region of the phase diagram. By increasing f_l/f_d, the peaks of the distributions turn down as long as they disappear. We see that several peaks in the distribution of avalanche sizes are obtained in Ref. [28]. The authors vary the convexity of the driving γ and the level of conservation ϵ in the isotropic case: $C=1$ when $\epsilon=0.25$. They find an intermediate region of the phase-diagram ϵ vs γ where the frequency-size distribution is characterized by peaks that scale with different powers of the system size L. Fixing the convexity of the driving γ ($\gamma=0$ for a uniform driving), for large values of the level of conservation, $C \geqslant 0.6$, the peaks disappear and they get a power-law decay with an exponential cutoff. Conversely, we find commensurate peaks in the FSO region in the whole range $C \in [0.4, 0.8]$.

We notice that an analysis of the anisotropic case of the OFC model is made in Ref. [27] where the authors introduce only two transfer coefficients $\alpha_1=f_l=f_r$ and $\alpha_2=f_u=f_d$ and control the degree of anisotropy by changing the ratio α_1/α_2, while keeping the level of conservation constant. They find that the anisotropy has almost no effect on the power-law exponent while the scaling exponent, expressing how the finite-size cutoff scales with the system size, changes continuously from a two-dimensional to a one-dimensional scaling of the avalanches [27]. Varying the anisotropic ratio α_1/α_2 in the range $[0,1]$ is equivalent to considering the straight line $f_u/f_d=1$ in the phase diagram of Fig. 7. As in Ref. [27], we find that on moving along the line $f_u/f_d=1$, the changes in the power-law exponent are negligible. However, differently Ref. [27], we find a crossover in the frequency-size distribution behavior from power-law to non-power-law (see Fig. 9). We attribute such a different result to the finite driving rate.

In conclusion, our analysis shows that only a finite range of values of the anisotropic transfer coefficients can supply

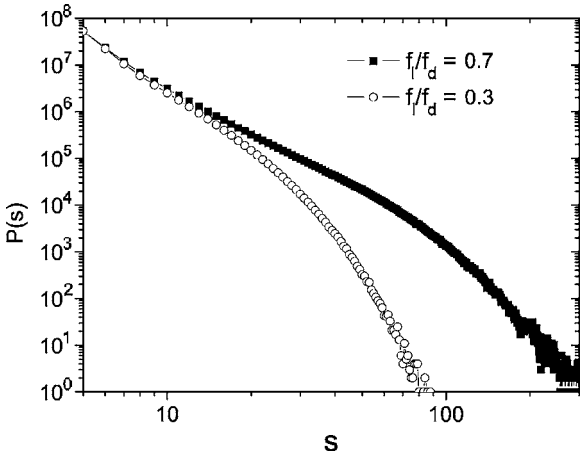

FIG. 9. Noncumulative frequency-size distributions on a 64 $\times 64$ grid for $f_u/f_d=1$ and $f_l/f_d=0.3$ (open dots) and $f_l/f_d=0.7$ (squares). The results are obtained for $\nu=10^{-4}$ and $C=0.4$.

power-law distributions. This characterization provides insight into the difficult determination of the complex and nonlinear transfer processes that occur in a landslide event.

V. CONCLUDING REMARKS

Explanation of the power-law statistics for landslides is a major challenge, both from a theoretical point of view and for hazard assessment. In order to characterize frequency-size distributions of landslide events, we have investigated a continuously driven anisotropic cellular automaton based on a dissipative factor of safety field. We have found that the value of the driving rate, which describes the variation rate of the factor of safety due to external perturbations, has a crucial role in determining landslide statistics. In particular, we have shown that, as the driving rate increases, the frequency-size distribution continuously changes from power-law to Gaussian shapes, offering the possibility to explain the observed rollover of the data for small landslides. The values of the calculated power-law exponents are in good agreement with the observed values. Moreover, the analysis of the model on varying the driving rate suggests the determination of correlated spatial domains of the factor of safety as a useful tool to quantify the severity of future landslide events.

As concerns the effects of anisotropic transfer coefficients, which control the nonconservative redistribution of the load of failing cells, we have found that the power-law behavior of the frequency-size distribution is a feature of the model only in a limited region of the anisotropy parameter space.

ACKNOWLEDGMENTS

E.P. wishes to thank A. Avella for stimulating discussions and a very friendly collaboration. This work was supported by MIUR-PRIN 2002/FIRB 2002, SAM, CRdC-AMRA, INFM-PCI, and EU MRTN-CT-2003-504712.

[1] Z. Olami, Hans Jacob, S. Feder, and K. Christensen, Phys. Rev. Lett. **68**, 1244 (1992).
[2] T. Simkin, Annu. Rev. Earth Planet Sci. **21**, 427 (1993).
[3] P. Bak, K. Chen, and C. Tang, Phys. Lett. A **147**, 297 (1992).
[4] R. Pastor-Satorras and A. Vespignani, Phys. Rev. E **61**, 4854 (2000).
[5] D. L. Turcotte, B. D. Malamud, F. Guzzetti, and P. Reichenbach, Proc. Natl. Acad. Sci. U.S.A. **99**, 2530 (2002).
[6] C. Dussauge, J. R. Grasso, and A. Helmstetter, J. Geophys. Res. **108**, 2286 (2003).
[7] P. Bak, *How Nature Works—The Science of Self-Organized Criticality* (Copernicus, Springer-Verlag, New York, 1996).
[8] P. Bak, C. Tang, and K. Wiesenfeld, Phys. Rev. Lett. **59**, 381 (1987); Phys. Rev. A **38**, 364 (1988).
[9] H. J. Jensen, *Self-Organized Criticality: Emergent complex behavior in physical and biological systems* (Cambridge University Press, Cambridge, England 1998).
[10] D. L. Turcotte, Rep. Prog. Phys. **62**, 1377 (1999).
[11] J. Faillettaz, F. Louchet, and J. R. Grasso, Phys. Rev. Lett. **93**, 208001 (2004).
[12] E. Piegari, V. Cataudella, R. Di Maio, L. Milano, and M. Nicodemi, Geophys. Res. Lett. **33**, L01403 (2006).
[13] D. Hamon, M. Nicodemi, and H. J. Jensen, Astron. Astrophys. **387**, 326 (2002).
[14] R. Dickman, A. Vespignani, and S. Zapperi, Phys. Rev. E **57**, 5095 (1998).
[15] D. Sornette, *Critical Phenomena in Natural Sciences, Chaos, Fractals, Self-organization and Disorder: Concept and Tools*, Springer Series in Synergetics (Springer-Verlag, Heidelberg, 2004).
[16] F. Brardinoni, and M. Church, Earth Surf. Processes Landforms **29**, 115 (2004).
[17] B. D. Malamud, D. L. Turcotte, F. Guzzetti, and P. Reichenbach, Earth Surf. Processes Landforms **29**, 687 (2004).
[18] S. Hergarten, Nat. Hazards Earth Syst. Sci. **3**, 505 (2003).
[19] L. Bjerrum, J. Soil Mech. Found. Div. **93**, 3 (1967).
[20] L. P. Kadanoff, S. R. Nagel, L. Wu, and S. M. Zhou, Phys. Rev. A **39**, 6524 (1989).
[21] R. Burridge and L. Knopoff, Bull. Seismol. Soc. Am. **57**, 341 (1967).
[22] K. Terzaghi, Geotechnique **12**, 251 (1962).
[23] D. G. Fredlund, and H. Rahardjo, *Soil Mechanics for Unsatured Soils* (Wiley-Interscience, New York, 1993).
[24] S. Hergarten and H. J. Neugebauer, Phys. Rev. E **61**, 2382 (2000).
[25] In order to visualize the S_i distribution, we introduced a lower threshold $e_{min}=10^{-3}$ and checked that the results do not change.
[26] L. Pietronero and W. R. Schneider, Phys. Rev. Lett. **66**, 2336 (1991).
[27] K. Christensen and Z. Olami, Phys. Rev. A **46**, 1829 (1992).
[28] A. Corral, C. J. Perez, A. Diaz-Guilera, and A. Arenas, Phys. Rev. Lett. **74**, 118 (1995).